GCA-TR-67-4-N

LABORATORY AND THEORETICAL INVESTIGATION OF CHEMICAL RELEASE EXPERIMENT

J. Pressman
P. Warneck
A. Sharma
J.P. Padur
H.K. Brown

FINAL REPORT

Contract ~~No~~ NASW-1341

GCA CORPORATION
GCA TECHNOLOGY ~~DIVISION~~
Bedford, Massachusetts

Febr~~uary~~ 1967

Prepared for

NATIONAL AERONAUTICS AND SPACE ADMINISTRATION
HEADQUARTERS
WASHINGTON, D.C.

TABLE OF CONTENTS

INTRODUCTION

This is the final report under NASA Contract No. NASw-1341, Laboratory and Theoretical Investigation of Chemical Release Experiments, 8 October 1965 - 10 November 1966. The purpose of this program was to perform both theoretical and laboratory studies which would support the field of chemical release experiments in the upper atmosphere. This involved measurements of rates, cross-sections, molecular spectroscopic factors, etc., and specific theoretical studies. A condensed Statement of Work of this contract is given below:

Statement of Work

Experimental. - Examine the chemiluminous reactions and make comparisons of the intensity of chemiluminous reactions between (a) atmospheric constituents of: (i) atomic oxygen, (ii) ozone and (iii) atomic nitrogen, and (b) organo-matallic compounds such as (i) trimethyl bismuth, (ii) trimethyl phosphorous, (iii) dimethyl mercury, (iv) diethyl cadmium or similar compunds.

Make measurements on relative intensities, reaction mechanisms and chemical consumption rates of compounds found suitable during former studies on chemical release experiments. Included among the compounds shall be (a) trimethyl antimony, (b) triethyl boron, (c) trimethyl aluminum, (d) diethyl zinc or similar compounds.

Examine the method of measurement of the atmospheric temperature from the study of fluorescence excited in intermediate species formed during the release of the compounds included in No. 2 above, or as mutually agreed between the parties hereto. Also, the fluorescence efficiency and the effect of ambient conditions of the observed temperatures shall be examined.

Conduct experiments directed toward the measurement, by differential spectrophotometry, of the ratios of active atmospheric species. The ratio of atomic oxygen to ozone through their chemiluminescence with nitric oxide and the ratio of atomic oxygen to atomic nitrogen through their chemiluminescence are among those contemplated.

Measure the deactivation of $O(^1D)$ by molecular oxygen for the purpose of elucidating the 6300Å atmospheric emission by release of oxygen into the atmosphere. The charge exchange cross-sections of O^+ with O_2 and N_2 shall be measured.

Theoretical. - Calculate necessary Franck-Condon factors and transition probabilities so as to ensure quantitative interpretations of intensity measurements.

Analyze for one of the compounds used in these studies the governing set of differential equations which can be used to determine its (compound) optical behavior under atmospheric release.

Study analytical techniques which are necessary for the differential spectrometric measurement of ratios of atmospheric active species.

Because of the detailed nature of the Quarterly Progress Reports on this program and the large number of technical and published papers, this Final Report will have the nature of a summary and review document. Since details can be obtained from the documents referred to, expensive, excessive, and cumbersome duplication can be avoided. Accordingly a list of contract highlights are furnished first and then a list of publications is given. Following this a review of the work performed and then a Summary of papers emanating from the program are reviewed. Where the material has been reported on in detail in the Quarterly Reports and the summary of the paper is reasonably full only a normal summary is furnished.

Summary Statement of Contract Highlights

Examination of the chemiluminous reactions of trimethyl bismuth, trimethyl phosphorous, dimethyl mercury and diethyl cadmium with atomic oxygen, atomic nitrogen and ozone.

Measurement of relative intensities of the foregoing compounds and in one instance the absolute intensity of the chemiluminescence of ozone with TMA.

The examination of the measurement of atmospheric temperature by the twilight fluorescence technique. Here analysis of previous measurements showed that the determination of relative vibrational transition probabilities were inconsistent. Consequently, new measurements were made. Further, the true potential energy curves for the A and X state of the AℓO molecule were computed. The vibrational wave functions of the different vibrational levels, the Franck-Condon factors and the r-centroids were also computed.

The deactivation of $O(^1D)$ by O_2 and the charge exchange cross section of O^+ with O_2 and N_2 has been measured.

A study of the optical morphology of chemical release clouds as a function of scattering angle for clouds of intermediate opacity (τ = 1-10) has been completed.

A study of the dynamic growth of particle clouds under conditions of various initial velocity distribution and drag laws has been completed.

A study has been made on the anomalous chemiluminescence rates observed for nitric oxide and atomic oxygen.

The fluorescence calculations and preliminary laboratory measurements of the vibrational transitions were checked in a simulator.

List of Publications

The following papers have been completed and submitted to scientific journals or are in preparation:

"A Spectroscopic Study of the Chemiluminescent Reaction of Germanium Tetrahydride with Atomic Oxygen," A. Sharma and J.P. Padur, submitted to Proc Phys Soc, accepted.

"The True Potential Energy Curves of $X^2\Sigma$ and $A^2\Sigma$ States of the AℓO Molecule," A. Sharma, accepted by J. Quant. Spectrosc. Rad. Trans.

"Franck-Condon Factors and R-Centroids of $A^2\Sigma$ and $X^2\Sigma$ Band System of A O," A. Sharma and P. Warneck, submitted to J. Quant. Spectrosc. Rad. Trans.

"Studies of Ion-Neutral Reactions by a Photoionization-Mass Spectrometer Technique," P. Warneck, favorably reviewed, second revision sent to J. Chem Phys.

"The Chemiluminescent Reactions of Atomic Oxygen with COS and H_2S", A. Sharma, J.P. Padur and P. Warneck, submitted to J. Phys. Chem., presented to AM. Chem. Soc. Mtg., September 1966, New York.

"Atmospheric Ion Neutral Reactions," P. Warneck, submitted to Planet. Space Sciences.

"The Morphology of Intermediate Optically Thick Vapor Atmosphere Clouds," J. Pressman and H.K. Brown, in preparation.

"The Dispersion of Particulate Matter in the Upper Atmosphere for Different Initial Velocity Distributions and Drag Laws," J. Pressman and H.K. Brown, in preparation.

"An Analysis of the Discrepancies of the Nitric Oxide-Atomic Oxygen Chemiluminescent Rate," A. Sharma and J. Pressman, in preparation.

"Spectroscopic and Fluorescent Studies of Chemiluminescent Reaction of Triethyl-Boron with Atomic Oxygen," A. Sharma, ShardaNand, and J.P. Padur, in preparation.

REVIEW OF WORK PERFORMED

De-activation of $O(^1D)$ by Molecular Oxygen and Nitrogen

Ozone production rates have been used as an indicator for presence of $O(^1D)$. This method is best used in conjunction with the photolysis of oxygen using 1470Å Xenon resonance radiation because at this wavelength the primary process is

$$(1) \quad O_2 + h\nu \rightarrow O + O^*$$

Where O^* signifies excited O-atoms in the ^1D states. At sufficiently high pressures of oxygen the subsequent reactions are

$$(2) \quad O + 2\,O_2 \rightarrow O_3 + O_2, \text{ fast}$$

$$(3) \quad O^* + O_2 + M \rightarrow O_2 + M, \; k_3$$

$$(4) \quad O^* + O_2 \rightarrow O_2 + O, \; k_4$$

$$(5) \quad O^* + O_3 \rightarrow O_2 + O_2, \; k_5$$

The determination of rate constants requires the quantitative measurement of the ozone quantum yield as a functionof various experimental parameters. However, as is generally true with photochemical systems, only ratios of rate constants can be determined and absolute rate constants must be obtained by comparison with other available values.

Briefly, the production of ozone in a flow system is investigated as a function of pressure and temperature and as a function of foreign gas admixture. Figure 1 shows the results obtained for pure oxygen, a 1:1 mixture of nitrogen and oxygen, and 1;4 mixture of nitrous oxide and oxygen, all at room temperature. The decline of the ozone quantum yield with decreasing pressure for pure oxygen and the oxygen-nitrogen mixture indicates qualitatively that quenching of $O(^1D)$ by either gas cannot be very rapid, since otherwise the ozone quantum yield should be independent of pressure and would have a value of $g(O_3) \approx 2$. The decrease of the ozone quantum yield to values of about unity in the N_2O-O_2 mixture indicates a complete loss of $O(^1D)$ by reaction with N_2O, which is known to be rapid.

A detailed analysis of these data will not be given here. The results can be expressed in terms of k_4/k_5, k_6/k_5 and k_7/k_5 where k_6 and k_7 are the rate coefficients associated with the reactions

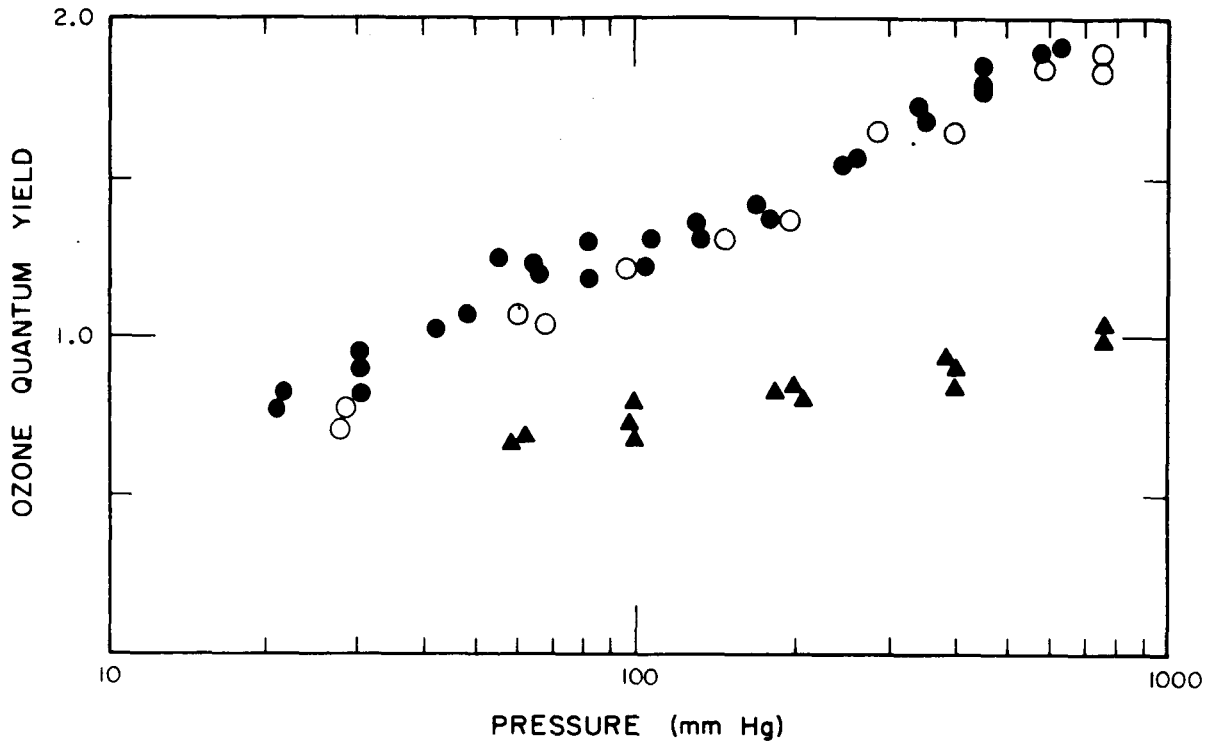

Figure 1. Ozone quantum yields as a function of pressure for a 4:1 mixture of oxygen with nitrous oxide (▲); and a 1:1 mixture of oxygen with nitrogen (○). Ozone quantum yields in pure oxygen are indicated by (●).

(6) $O^* + N_2 \rightarrow O + N_2$

(7) $O^* + N_2O \rightarrow N_2 + O_2$

$\rightarrow NO + NO$

The partitioning ratio for the two types of reation products in Reaction (7) are about 1:1. The resulting rate constant ratios are shown below

k_4/k_5	k_6/k_5	k_7/k_5
6.1×10^{-4}	2.7×10^{-4}	6.0×10^{-3}

It is evident that in all cases the reaction of $O(^1D)$ with ozone is much faster. A lower limit for k_5 has been given by Fitzsimmons and Bair from data concerning the flash photolysis of ozone. An upper limit to k_5 can be obtained from the temperature dependence of the ozone quantum yield in the present work which has been reported elsewhere. Thus, $k_5 \approx 7 \times 10^{-12}$ cc/molecule second. The absolute rate constant for the deactivation by oxygen is, accordingly, $k_4 \approx 4 \times 10^{-15}$ cc/molecule second. The other rate constants are $k_6 \approx 2 \times 10^{-15}$ cc/molecule second, $k_7 \approx 4 \times 10^{-14}$ cc/molecule second.

Ion-Molecule Reactions

The general nature of this study is described in the summaries of the publications in next section where some of the values of the rate coefficients are furnished. Details of the apparatus and experimental conditions are furnished in the Third Quarterly Report.

Rate constants determination are described here for the reaction of nitrogen ions with oxygen and nitrogen, (1) and (2). That for (3) and (4) are omitted in this summary. More specifically, these reactions are:

(1) $N_2^+ + O_2 \rightarrow O_2^+ + N_2$

(2) $N_2^+ + O_2 \rightarrow NO^+ + NO$

(3) $N_2^+ + N_2 \rightarrow N_4^+$

(4) $H_2^+ + H_2 \rightarrow H_3^+ + H$

The above reactions were studied with radiation centered at 764Å wavelength. Owing to the limited wavelength resolution, the employed radiation contained several component lines, the three strongest being NIV 765.1, NIII 764.4, and

OV 760.4Å. The associated energy spread is 0.1 eV. The available photon energy lies 0.64 eV above the threshold for N_2^+ formation and 0.75 eV above that for H_2^+ formation. Although this is insufficient for the production of ions in electronically excited states, it includes the excitation of vibrational or rotational levels. Specifically, for H_2^+, the occurrence of vibrational excitation has been demonstrated in this wavelength region.

Reactions (1) and (2) were studied with air introduced inthe system at source pressures up to 200 microns. Reaction (1) proceeded rapidly while Reaction (2) was negligible under all condition. Figure 2 shows the N_2^+ and O_2^+ ion currents observed as a function of pressure for a repeller voltage setting of 0.5 volt. Occurrence of Reaction (1) is evidenced by the rise of O_2^+ current at the expense of the N_2^+ current. Also shown in Figure 2 is the sum of both currents which, in this case, exhibit an almost linear pressure dependence. The deviations from linearity are attributable to the increase of light absorption in the source. The limiting ratio of the ion currents at low pressures, $R = i(N_2^+)/i(O_2^+)$, was determined by expansion of Figure 2 as R = 7.1. The ratio expected from the known absorption and photionization coefficients, taking into account only the three strongest lines contributing to the radiation, weighed according to their intensity, is R = 8.5. The agreement is reasonable if it is considered that the wavelength setting may have favored either one of the outer lines of this group.

Rate constants determined from the data shown in Figure 2 are given in Table 1.

TABLE 1

RATE CONSTANTS FOR THE REACTION $N_2^+ + O_2$

microns	(N_2^+)	(O_2^+) (arbitrary units)	$(O_2^+)_o$ (arbitrary units)	$(O_2^+)_o$	τ μsec	$\log \frac{(N_2^+)_o}{(N_2^+)_o - \Delta(O_2^+)}$	k x 10^{10} cc/molecule sec
41	370	81	396	55	2.6	0.031	1.01
60	490	156	566	80	3.8	0.063	0.96
87	565	310	766	108	5.6	0.134	0.96
100	560	415	854	120	6.8	0.184	0.94
114	550	600	1007	142	7.6	0.263	1.06
123	508	662	1025	144	8.4	0.305	1.22
135	498	830	1162	163	9.6	0.370	0.99
140	450	930	1208	170	10.0	0.431	1.07
149	452	956	1232	173	10.4	0.439	0.99
160	367	1135	1315	185	11.2	0.554	1.07
168	320	1355	1465	207	11.6	0.665	1.19
170	302	1215	1355	191	11.8	0.612	1.06
190	260	1600	1629	239	12.8	0.783	1.12
192	236	1638	1640	231	12.9	0.868	1.22

average $k_1 = 1.06 \times 10^{-10}$ cc/molecule sec

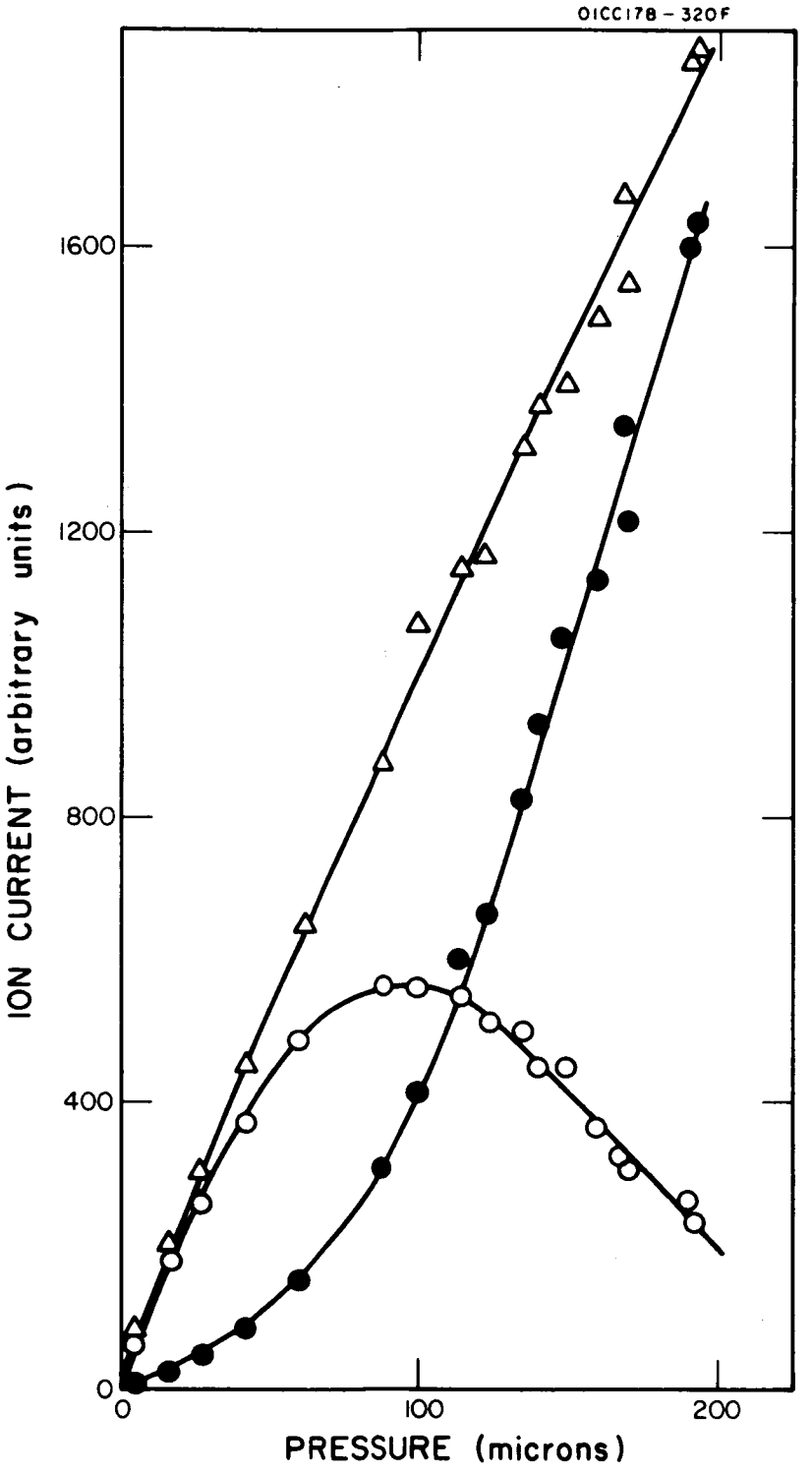

Figure 12. Mass 28 (O) and mass 32 (●) ion currents as a function of ion source pressure. Sum of ion currents indicated by triangles.

Chemiluminescence in the Reactions of Atomic Oxygen Watt COS and H_2S

Mass spectrometric investigations by Liuti, Dondes, and Harteck [Ref. 1] and in this laboratory [Ref. 2] have shown that the first step in the reaction of oxygen atoms with carbonyl sulfide is the formation of SO radicals

$$(1) \quad O + COS \rightarrow CO + SO$$

The rate constant for this process has been determined [Ref. 2]. The reaction of oxygen atoms with hydrogen sulfide has also been found [Ref. 1] to yield SO radicals via

$$(2) \quad O + H_2S \rightarrow H_2 + SO$$

although there is probably a second operative reaction path leading to OH and SH radicals as additional products.

The chemiluminescence associated with these reactions has also been investigated [Ref. 3-7]. A comparative study [Ref. 3] has shown that the emission spectra from the reactions of oxygen atoms with carbonyl sulfide, hydrogen sulfide and carbon disulfide, and the SO_2 afterglow spectrum are nearly identical, featuring similar intensity distributions. These observations suggest that the emitter and the process leading to the formation of the emitter are the same in all four cases of chemiluminescence. Evidence is mounting that the reaction responsible for the emissions is

$$(3) \quad O + SO \rightarrow SO_2 + h\nu$$

as was originally suggested by Gaydon [Ref. 4]. Hermann, et al., [Ref. 5] observed that the short wavelength cut-off of the SO_2 afterglow near 2400Å coincides with the onset of the dissociation continuum in the SO_2 absorption spectrum. Halstead and Thrush [Ref. 6] found that the SO_2 afterglow intensity is directly proportional to the product of oxygen atom and SO radical concentrations. More recently, Rolfes, Reeves, and Harteck [Ref. 7] studied the light emission from the reaction of O-atoms with COS at low total pressures, and compared with with the $O + NO_2$ reaction resulting in the air afterglow emission involving radiative combination of atomic oxygen with nitric oxide. Their results indicate that the two reactions are analogous and that reaction (3) proceeds via a simple two-body combination mechanism.

The present work set out to derive additional evidence for the occurrence of Reaction (3) by studying the time dependence of the chemiluminescent intensity in the reactions of atomic oxygen with COS and H_2S for various initial reactant concentrations. From such experiments, the rate coefficients associated with Reactions (2) and (3) could be determined. In addition, intensity profiles

* Numbers in [ ] denote references

were obtained for the later stage of the reaction of oxygen atoms with COS to explore the possibility of other SO loss reactions besides Reaction (3).

The behavior of chemiluminescence intensity with reaction time and reactant concentrations in the initial stage of the Reactions (1) O + COS and (2) O + H_2S has been found to support the suggestion that the reaction responsible for the chemiluminescence is the radiative combination of atomic oxygen with SO radicals: Reaction (3). Comparative intensity measurements enabled the determination of the rate constants associated with Reactions (2) and (3). The combination Reaction (3) was found to be almost as fast as Reactions (1) and (2), so that it causes an appreciable consumption of SO radicals in the later stages of the reactions. Nevertheless, an additional SO loss reaction is required to explain the intensity profiles observed in the later reaction stages.

The values of the rate coefficients consistant with this experimetric program are

$$k_1 = 0.91 \times 10^{-14} \text{ cc/molecule sec}^2$$

$$k_2 = 1.70 \times 10^{-14} \text{ cc/molecule sec}^2$$

$$k_3 = 5.7 \times 10^{-15} \text{ cc/molecule sec}^2$$

Chemiluminescence Reaction of Germanium with Atomic Oxygen

This study is summarized in the next section, and details were given in the Third Quarterly Report. The spectroscopic studies of the chemiluminous reactions of atomic oxygen with several substances have been previously undertaken by several workers and summarized by Gaydon [Ref. 8]. Recently, Kaufman [Ref. 9] has reviewed the kinetics of the atomic oxygen reactions with various compounds. However, no information regarding the chemiluminescent reaction of atomic oxygen with germanium compounds is available. We have found that the reaction of germanium tetrahydride with atomic oxygen is accompanied by a strong blue chemiluminescence. On the other hand, we did not observe any visible chemiluminescence during the reaction of atomic oxygen with garmanium tetrachloride.

The examination of the spectra of the chemiluminescence produced during the reaction of germanium tetrahydride and atomic oxygen reveals a large number of bands in the region from 2450 to 5100Å. Most of the bands on the short wavelength side of the spectrum belong to the D-X system of GeO. In addition to the bands of the D-X system of GeO observed by previous investigators, we have observed a number of new bands belonging to the above system. A number of unidentified bands are also observed, which presumably indicate the presence of a new band system of the GeO molecule on the longer wavelength side of the D-X system of GeO. In this summary, we shall present the results of the spectroscopic

study of the chemiluminescent reaction of germanium tetrahydride and atomic oxygen. In Table 2 and Figure 3 are presented the spectrum observed.

The True Potential Energy Curves of $X^2\Sigma$ and $A^2\Sigma$ States of the AℓO Molecule

The $A^2\Sigma$ - $X^2\Sigma$ band system for AℓO is of considerable astrophysical and geophysical importance. For example, the relative intensity of the bands belonging to the $A^2\Sigma$ - $X^2\Sigma$ system of AℓO observed [Ref. 11-13] during the rocket release of aluminum compounds in the upper atmosphere at twilight have been used to obtain information regarding upper atmospheric temperatures. The interpretation of such experiments requires information concerning relative vibrational transition probabilities and Franck-Condon factors. The Franck-Condon factors for the above band system have been calculated by Nicholls [Ref. 14] and Tawde et al., [Ref. 15] after assuming that the $A^2\Sigma$ and $X^2\Sigma$ states of AℓO follows the Morse curve. Zare et al., [Ref. 16] have shown that, in certain cases, the Franck-Condon factors are quite sensitive to the shape of the potential energy curves. Therefore, the true potential curves of the $A^2\Sigma$ and $X^2\Sigma$ states of AℓO are calculated and compared with the Morse potential. These data are displayed in Figures 4 and 5.

The Franck-Condon Factors and r-centroids of the $A^2\Sigma$ - $X^2\Sigma$ Band System of AℓO*

The relative intensity of the bands belonging to the $A^2\Sigma$ - $X^2\Sigma$ system of AℓO observed [Ref. 17-19] during the rocket release of aluminum compounds in the upper atmosphere at twilight have been used to obtain information regarding upper atmospheric temperature. The interpretation of the relative intensities of bands require information concerning Franck-Condon factors and r-centroids. The Franck-Condon factors and r-centroids of the above band system have been calculated by Nicholls and Tawde et al., after assuming that [Ref. 20 and 21] the $A^2\Sigma$ and $X^2\Sigma$ states of AℓO follow the Morse curve. However, Sharma [Ref. 22] calculated the RKR potentials of the $A^2\Sigma$ and $X^2\Sigma$ states of AℓO and compared them with the corresponding Morse potentials. He concluded that the potential energy curve of the $X^2\Sigma$ state can be reasonably represented by the Morse curve, but that the deviation of the true potential for the $A^2\Sigma$ state from the corresponding Morse potential is appreciable even for lower vibrational levels.

It may be noted that Zare et al., [Ref. 23] have shown that for major band systems of N_2, the difference between the Franck-Condon factors calculated from RKR potential and those calculated from Morse potential may be as much as 20 percent for strong transitions [$q(\nu',\nu'') \geq 0.01$]. Therefore, the Franck-Condon factors and r-centroids for the $A^2\Sigma$ - $X^2\Sigma$ system of AℓO are calculated from the true potential energy curves of the two states given by Sharma [Ref. 22] and are reported here. The Franck-Condon factors are given in Table 3 and the r-centroid in Table 4.

TABLE 2

THE IDENTIFICATION OF THE BANDS OF D-X SYSTEM OF GeO

Measured λ Å	Intensity Visual Estimate	(λ(v′,v″) [Ref. 10]	Identification λ Calculated (v′,v″)
2364.7*	1		2365.85 (11,2)
2373.6*	1		2375.4 (9, 1)
2386.1*	2		2385.67 (7, 0)
2397.1*	2		2398.3 (10,2)
2406.8*	2		2408.29 (8, 1)
2418.9*	6		2419.85 (6, 0)
2429.4*	1		2431.33 (9, 2)
2441.40	10	2441.9 (7, 1)	2442.61 (7, 1)
2454.0	12	2454.8 (5, 0)	2454.80 (10,3), 2455.52 (5, 0)
2465.1*	4		2465.81 (8, 2)
2477.3	5	2477.8 (6, 1)	2478.45 (6, 1)
2491.5	18	2492.2 (4, 0)	2489.43 (9, 3), 2492.80 (4, 0)
2501.9*	2		2501.80 (7, 2)
2514.8	10	2514.88 (5, 1)	2513.50 (10,4), 2515.89 (5, 1)
2430.0	30	2531.10 (3, 0)	2531.76 (3, 0)
2562.4*	1		2563.35 (7, 3)
2571.0	30	2571.83 (2, 0)	2572.52 (2, 0)
2587.6*	2		2587.76 (8, 4)
2602.8*	12		2602.85 (6, 3)
2613.5	30	2514.13 (1, 0)	2612.62 (9, 5), 2615.20 (1, 0)
2621.90	15	2619.5 (4, 2)	2619.36 (4, 2)
2627.8*	6		2627.4 (7, 4)
2638.0	12	2639.17 (2, 1)	2637.9 (10,6), 2638.85 (2, 1)
2644.9*	12		2644.17 (5, 3)
2652.2*	1		2652.46 (8, 5)
2658.5	20	2659.42 (0, 0)	2659.90 (0, 0)
2661.1	20	2662.33 (3, 2)	2662.93 (3, 0)
2682.2	30	2682.98 (1, 1)	2683.78 (1, 1)
2713.4	4	2707.4 (2, 2)	2712.40 (5, 4)
2720.4*	2		2719.85 (8, 6)
2730.17	20	2730.02 (0, 1)	2730.90 (0, 1)
2754.6*	15		2755.4 (1, 2)
2780.1	15	2779.71 (2, 3)	2780.55 (2, 3)
2804.2	20	2804.17 (0, 2)	2805.09 (0, 2), 2805.73 (3, 4)
2837.4*	15		2836.25 (7, 7)
2845.9*	4		2844.3 (10,9)
2856.2	15	2855.42 (2, 4)	2855.87 (2, 4), 2857.89 (5, 6)
2881.6	30	2881.75 (0, 3)	2881.95 (3, 5), 2882.71 (0, 3)
2893.8*	5		2890.93 (9, 9)
2907.5	16	2908.1 (1, 4)	2908.57 (1, 6), 2908.80 (4, 6)

TABLE 2 (continued)

Measured λ Å	Intensity Visual Estimate	(λ(v′,v″) [Ref. 10]	Identification λ Calculated (v′,v″)
2919.3*	2		2919.0 (10,10)
2961.8	20	2963.04 (0, 4)	2961.68 (3, 6), 2963.99 (0, 4)
2969.6*	5		2968.13 (9,10)
2988.9	30	2989.89 (1, 5)	2988.89 (4, 7), 2990.56 (1, 5)
3016.5*	10		3016.73 (5, 8), 3017.61 (2, 6)
3048.8	5	3048.76 (0, 5)	3047.8 (9,11), 3048.76 (0, 5)
3075.5	25	3075.7 (1, 6)	3073.81 (7,10), 3073.18 (4, 8)
			3076.51 (1, 6)
3104.2	16	3103.1 (2, 7)	3104.31 (2, 7), 3103.4 (8,11)
3132.4	4	3131.6 (3, 8)	3132.62 (3, 8)
3134.3*	4		3133.1 (9,12)
3139.0*	1		3138.58 (0, 6)
3158.3*	2		3158.6 (7,11)
3166.1	12	3165.9 (1, 7)	3166.67 (1, 7)
3196.2	12	3194.3 (2, 8)	3195.26 (2, 8)
3221.0	30	3222.9 (3, 9)	3221.3 (9,13), 3224.36 (3, 9)
			3220.8 (6,11)
3248.7*	8		3251.0 (7,12), 3252.6 (10,14)
			3253.98 (4,10)
3262.2*	6		3261.37 (1, 8)
3291.0	6	3289.7 (2, 9)	3290.76 (2, 9)
3312.4*	1		3313.6 (9,14), 3314.8 (6,12)
3320.8	15	3319.4 (3,10)	3320.69 (3,10)
3324.3*	20		3331.21 (0, 8)
3352.3*	15		3349.2 (4,11)
3380.2*	6		3378.0 (8,14), 3382.0 (5,12)
3412.5*	1		3410.4 (9,15), 3413.7 (6,13)
3422.0*	4		3421.0 (3,11)
3436.9*	6		3435.15 (0, 9)
3454.3*	3		3453.3 (4,12)
3463.4*	8		3465.72 (1,10)
3484.7*	1		3485.2 (5,13)
3490.8*	8		3494.6 (2,11)
3519.2*	6		3517.6 (6,14)
3592.8*	1		3593.5 (5,14)
3610.5*	2		3608.2 (2,12)
3638.6*	3		3640.8 (3,13)
3794.4*	1		3793.3 (4,15)
3812.7*	2		3815.8 (1,13)

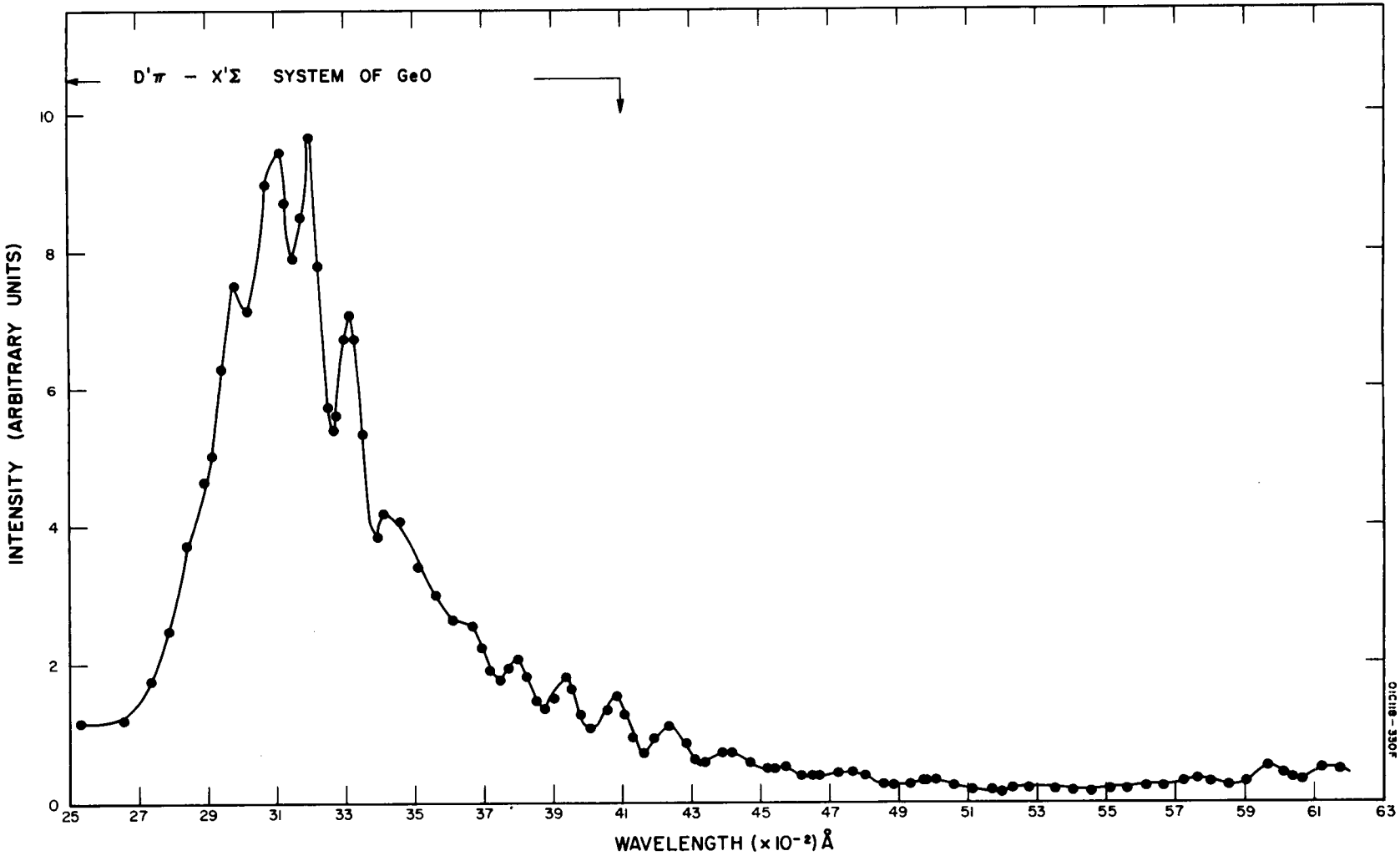

Figure 3. The corrected spectrum of the chemiluminescence produced during the reaction of germanium tetrahydride with atomic oxygen.

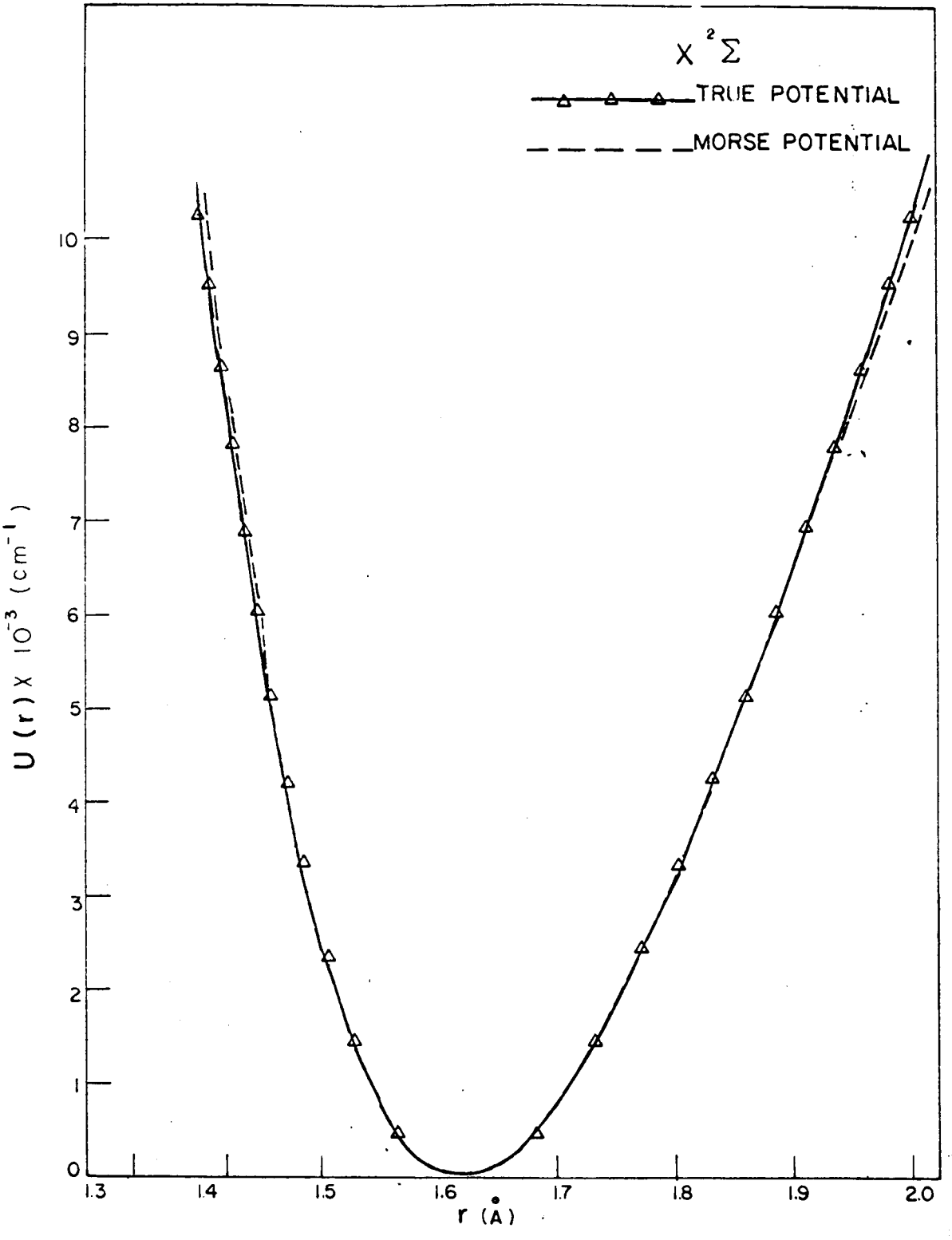

Figure 4. True potential curves of the $X^2\Sigma$ states of AlO calculated and compared with the Morse potential.

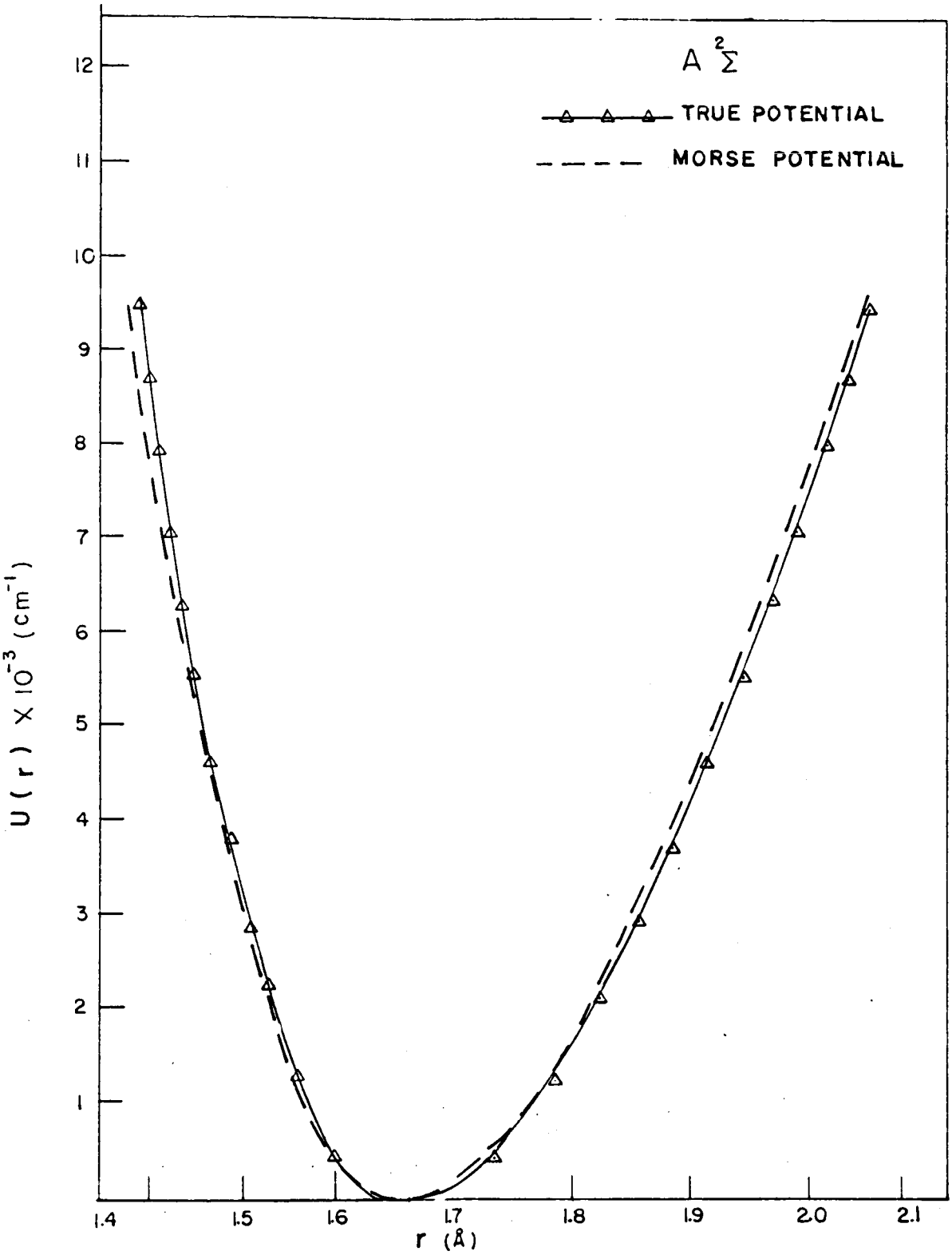

Figure 5. True potential curves of the $A^2\Sigma$ states of AℓO calculated and compared with the Morse potential.

TABLE 3

FRANCK-CONDON FACTORS OF $A^2\Sigma$-$X^2\Sigma$ BAND SYSTEM OF AℓO MOLECULE

v′ \ v″	0	1	2	3	4	5	6	7	8	9
0	*7.297-1	2.366-1	3.174-2	1.904-3	2.990-5	6.949-8	7.678-9	8.160-10	5.946-9	6.078-10
	†7.298-1	2.379-1	3.070-2	1.577-3	1.968-5	8.992-8	1.818-8	7.104-12		
1	2.233-1	3.457-1	3.493-1	7.567-2	5.873-3	1.131-4	2.918-7	4.340-11	8.117-10	2.356-8
	2.244-1	3.565-1	3.428-1	7.147-2	4.685-3	5.590-5	9.332-7	9.212-8		
2	4.065-2	3.026-1	1.389-1	3.842-1	1.217-1	1.159-2	2.406-4	1.325-6	1.003-7	1.249-8
	4.024-2	3.006-1	1.604-1	3.776-1	1.124-1	8.685-3	8.681-5	4.430-6		
3	5.563-3	9.352-2	2.978-2	4.169-1	3.769-1	1.657-1	1.846-2	3.723-4	4.372-6	4.509-7
	5.037-3	8.794-2	3.038-1	6.320-2	3.777-1	1.494-1	1.282-2	8.953-5		
4	6.445-4	1.845-2	1.381-1	2.568-1	5.242-3	3.497-1	2.047-1	2.587-2	4.724-4	1.253-5
	2.000-5	1.695-3	2.900-2	1.589-1	2.363-1	3.215-3	3.447-1	2.073-1		
5	7.013-5	2.762-3	3.623-2	1.684-1	2.044-1	8.923-4	3.154-1	2.381-1	3.320-2	5.105-4
	2.000-5	1.695-3	2.900-2	1.589-1	2.363-1	3.215-3	3.447-1	2.073-1		
6	7.352-6	3.448-4	6.741-3	5.607-2	1.846-1	1.526-1	1.168-2	2.807-1	2.266-1	4.005-2
	3.843-8	9.946-5	3.970-3	4.422-2	1.777-1	1.975-1	9.659-6	3.277-1		
7	5.443-7	3.760-5	9.830-4	1.267-2	7.600-2	1.879-1	1.079-1	2.792-2	2.488-1	2.911-1
	2.304-7	4.468-7	2.848-4	7.219-3	5.926-2	1.875-1	1.632-1	1.997-3		
8	1.221-9	3.128-6	1.191-4	2.180-3	2.044-2	9.372-2	1.815-1	7.236-2	4.466-2	2.213-1
	2.206-8	7.177-8	1.201-5	3.045-4	4.102-3	2.948-2	1.080-1	1.685-1	4.563-2	5.945-2

* $q_{v'v''}$ calculated from RKR potentials.
† $q_{v'v''}$ calculated from Morse potential.

The negative number in each entry is the power of ten by which it is multiplied.

TABLE 4

r-CENTROIDS(Å) OF $A^2\Sigma$-$X^2\Sigma$ SYSTEM OF AℓO MOLECULE

v′ \ v″	0	1	2	3	4	5	6	7	8	9
0	*1.647	1.728	1.812	1.918	2.166	0.5621	1.227	1.795	1.663	1.402
	†1.646	1.727	1.813	1.937	2.215					
	‡1.65	1.73	1.85	>2						
1	1.575	1.658	1.738	1.825	1.938	2.184	0.5853	1.736	1.234	1.624
	1.574	1.657	1.739	1.826	1.957	2.295				
	1.58	1.65	1.74	1.85	>2					
2	1.507	1.583	1.671	1.749	1.837	1.956	2.220	0.9608	2.333	1.351
	1.505	1.580	1.669	1.752	1.839	1.979	2.411			
	1.50	1.59	1.66	1.76	1.88	>2				
3	1.436	1.516	1.590	1.693	1.761	1.849	1.974	2.277	1.233	2.222
	1.429	1.511	1.586	1.685	1.765	1.852	2.003	2.606		
	1.43	1.50	1.59	1.67	1.76	1.88	>2			
4	1.364	1.448	1.524	1.598	1.758	1.773	1.862	1.992	2.352	1.441
	1.326	1.436	1.517	1.591	1.713	1.779	1.866	2.030		
		1.45	1.51	1.60	1.68	1.77	1.89	>2		
5	1.300	1.376	1.457	1.531	1.605	1.451	1.786	1.874	2.011	2.452
		1.336	1.443	1.522	1.596		1.794	1.881		
			1.44	1.52	1.62	1.68	1.77	1.89	>2	
6	1.243	1.299	1.386	1.465	1.537	1.611	1.616	1.800	1.887	2.031
			1.346	1.449	1.527	1.600		1.809		
				1.47	1.53	1.61	1.69	1.77		
7	1.119	1.220	1.306	1.396	1.473	1.543	1.618	1.642	1.815	1.900
				1.354	1.454	1.531				
					1.48	1.54	1.62	1.59		
8	1.878	1.095	1.217	1.318	1.405	1.479	1.549	1.625	1.653	1.831
						1.48	1.55	1.63		
9	1.817	0.407	1.107	1.229	1.330	1.413	1.486	1.554	1.633	1.660
							1.48	1.56		

* Calculated from RKR potential † Calculated from Morse potential ‡ Graphical method

Relative Vibrational Transition Probability of $A^2\Sigma - X^2\Sigma$ Band System of AℓO

In order to obtain reliable values of vibration transistion probability the accurate measurements of the relative intensity and the calculated Franck-Condon factors should be available. Tawde and Trivedi [Ref. 24] first measured the relative intensity of the AℓO bands belonging to the $A^2\Sigma - X^2\Sigma$ system. They used the peak intensity method for obtaining the relative intensity of the observed bands. This method is similar to the fractional band intensity method discussed by Robinson and Nicholls [Ref. 25]. The above methods assume that the intensity of the band head is proportional to that of the whole band. Since the above assumption is of limited validity, Tawde and Korwar [Ref. 26] have remeasured the relative total intensity of the bands of AℓO blue green system excited in a dc arc between pure aluminum electrode at 220V and 2 amp current. Moreover Herbert and Tyte [Ref. 27] have measured the relative intensity of the bands of the above system excited in an aluminum arc operated at 30 cm Hg of air pressure and 600V ac with 300 mA current. However, Tyte and Herbert [Ref. 28] have also measured the relative intensity of the bands belonging to the $A^2\Sigma - X^2\Sigma$ system of AℓO excited in hydrogen driven shock wave through argon containing 10 percent oxygen and aluminum poder and also in exploding aluminum foil in air at 400 cm Hg pressure. Furthermore, the relative intensity measurement of the bands of the above system of AℓO observed in the spectrum of the glow produced during the twilight explosive release of aluminum containing charges in the upper atmosphere by Harang [Ref. 29] are also available. The measurements of the relative intensities are summarized in Table 5. The consistency of the above intensity measurements can be tested as follows: The intensity of a band in emission is given:

$$I = (\nu', \nu'') = DN(\nu')\, E^4(\nu', \nu'')\, R^2(\bar{r}, \nu', \nu'')\, g(\nu', \nu'') \qquad (1)$$

The relative intensity of the two bands belonging to the same ν''-progression originating from the same ν' levels but terminating at different ν'' levels ν_1'', and ν_2'' should be given by,

$$\frac{I(\nu', \nu_1'')}{I(\nu', \nu_2'')} = \frac{E^4(\nu', \nu_1'')\, R_e^2(\bar{r}, \nu', \nu_1'')\, q(\nu', \nu_1'')}{E^4(\nu', \nu_2'')\, R_e^2(\bar{r}, \nu', \nu_2'')\, q(\nu', \nu_2'')} \qquad (2)$$

Equation (2) shows that the relative intensity of the bands belonging to the same ν''-progression should be the same in different sources. An examination of Table 5 shows that there is large variations in the reported relative intensities of the bands belonging to the same ν'' progression, which may be due to: (1) The presence of background radiation in the observed spectrum, and (2) the self absorption by AℓO vapor. The presence of background radiation in the observed spectrum if present with substantial intensity can be detected and appropriate corrections can be made.

TABLE 5

λ	v′,v″	ac Arc [Ref. 12]	Exploding Aℓ Foil [Ref. 28]	Shock Tube [Ref. 28]	dc Arc [Ref. 26]	Explosive Release [Ref. 29]
4842.2	0,0	100	100	100	100	100
5079.4	0,1	9.4	38.4	23.0	13.7	31.0
5337.0	0,2	0.5	1.1	1.2	--	--
4648.1	1,0	17.6	53.8	35.2	20.9	21.7
4866.2	1,1	14.2	56.8	20.6	30.5	26.3
5102.0	1,2	13.8	49.4	36.6	28.8	20.9
5337.8	1,3	1.1	1.5	3.3	--	--
4470.4	2,0	0.7	24.8	4.8	--	--
4671.9	2,1	25.1	51.6	29.4	30.7	13.3
4888.8	2,2	3.9	30.2	4.3	15.2	3.8
5123.1	2,3	12.3	38.3	24.3	41.0	9.3
5376.9	2,4	1.9	2.4	6.0	--	--
4493.8	3,1	4.2	28.2	11.9	7.4	--
4694.4	3,2	12.6	35.4	19.7	40.9	4.7
5142.6	3,4	6.7	30.0	13.7	55.0	3.1
5394.2	3,5	1.0	3.3	6.0	--	--

However, the self absorption effects are not so apparent, and the previous workers have not investigated the effect of self absorption onthe observed relative intensities of the AℓO bands. It may be noted that since the lower state of the above band system is the ground state of AℓO molecule, the observed relative intensities can be seriously affected by self absorption. GCA in the Table 5 has pointed up this in consisting and has made additional measurements of AℓO spectra under a variety of conditions: arcs, discharges, and lower exactation. This data is presently being evaluated.

The Morphology of Intermediate Optically Thick Chemical Release Clouds

Some of the results of this study are presented here while the rationale and methodology of this theoretical study is presented in the paper summary in the next section. Figure 6 shown some of the different images that can be achieved depending upon the optical thickness and the phase angle (the angle between the direction of illumination and viewing). Figure 7 shows a specific picture made from the simple graphical technique involved in this study of the visual image.

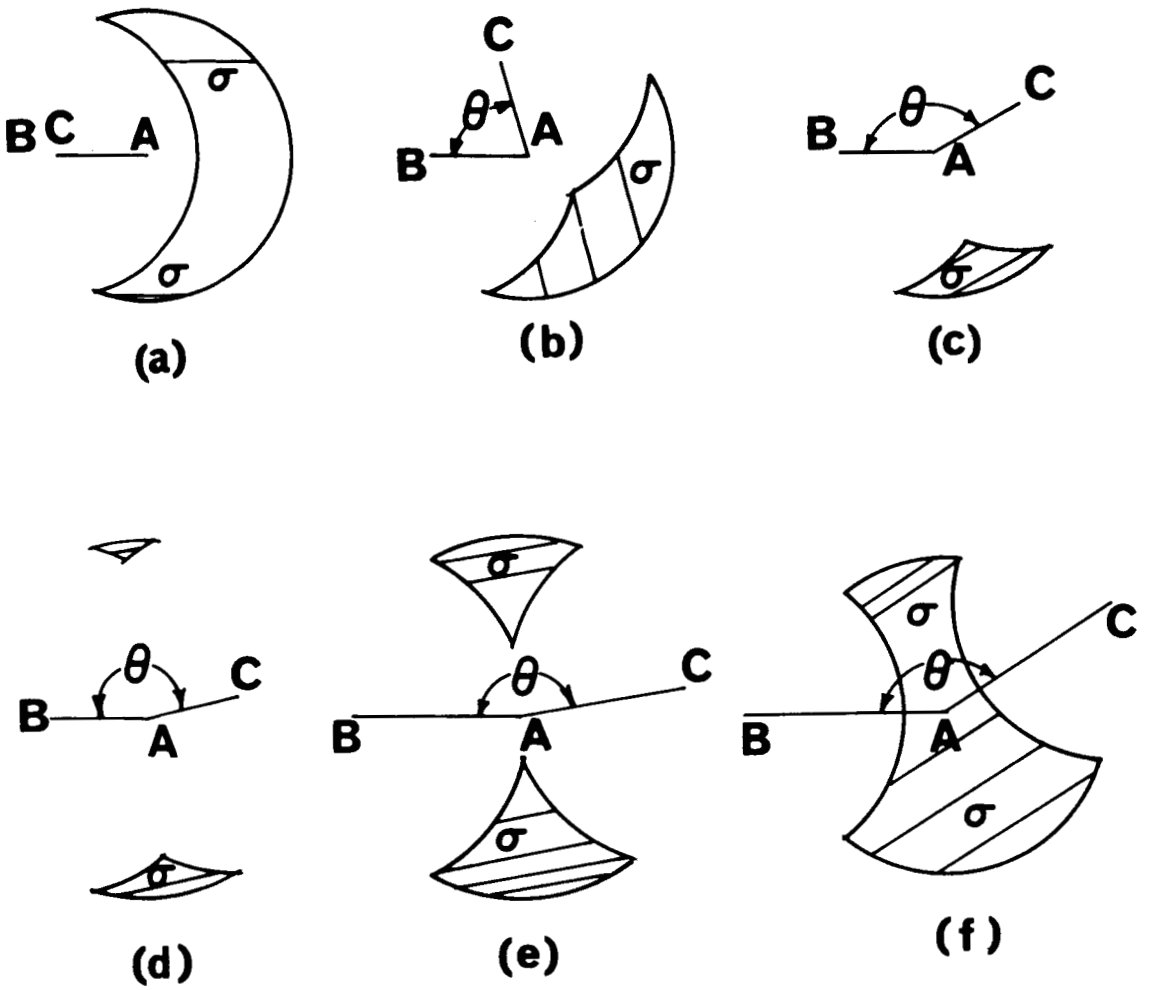

Figure 6. Sketches of typical shapes of the circular arc region of definition of $\sigma = \sigma(\eta, r, \theta)$.

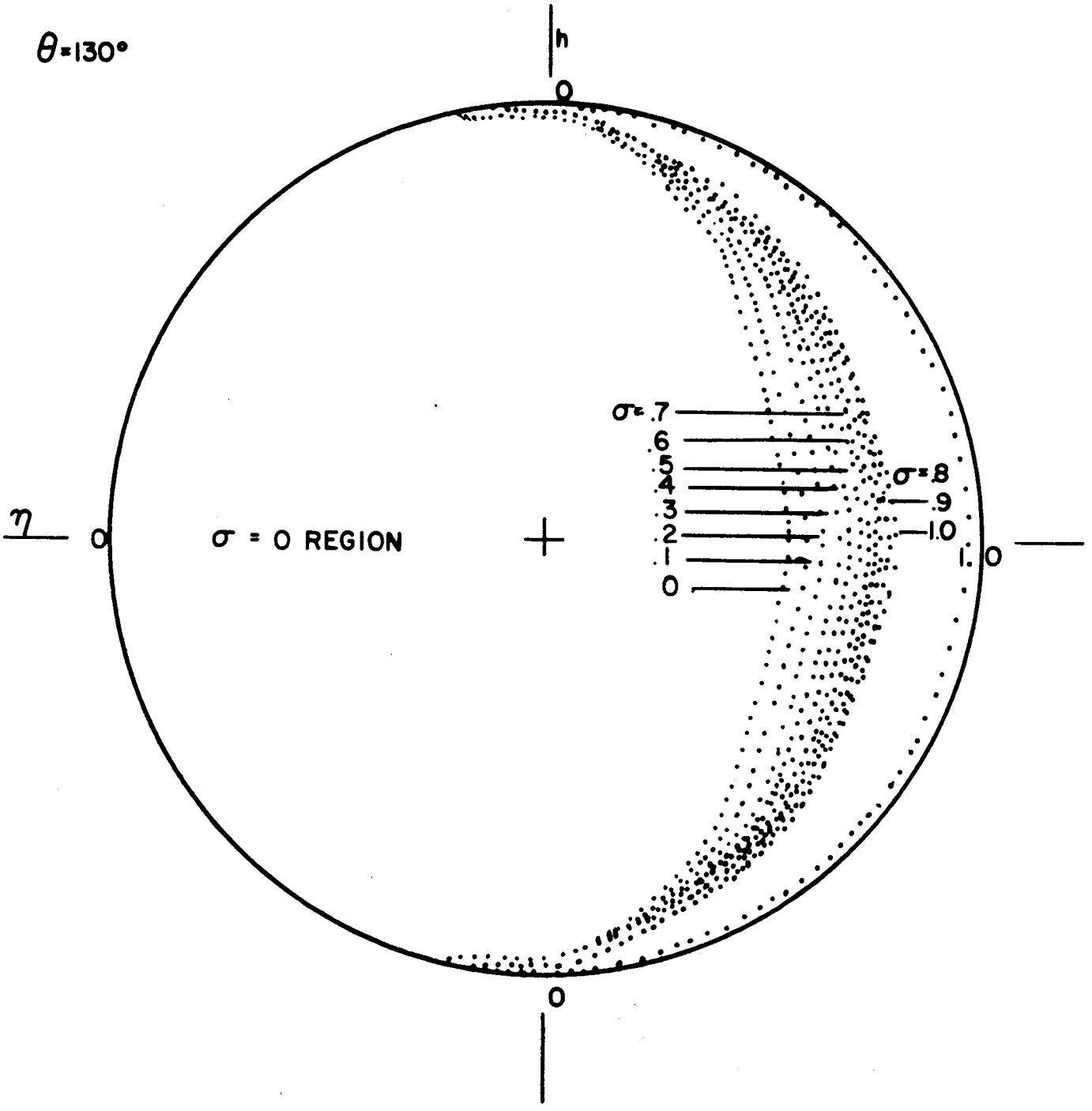

Figure 7. Plane image of photoluminescent homogeneous spherical cloud as seen by an observer at an angle $\theta = 130^{\circ}$ with the sun, showing isophote curves $\sigma(\eta,h,\theta) = \text{constant}$; optical depth $\sigma_e = 1$, radius of sphere $R = 4$.

Conversion of Velocity Distribution to Density Distribution

The purpose of this section is to establish the density distribution of particle released in the oxygen atmosphere for various initial velocity distributions under various types of drag conditions typical of a given altitude. Only monodisperse particle are considered.

Maxwell Distribution. -

(a) Free Expansion with No Drag. - This case is described by the initial velocity distribution

$$\delta N = N \left(\frac{1}{\pi \, v_M^2} \right)^{3/2} 4 \pi v^2 \exp \left(- \frac{v^2}{v_M^2} \right) \delta v \tag{3}$$

where

$v_M = (2kT/M)^{1/2}$ and the resulting density distribution is:

$$\rho(r,t) = N \left(\frac{1}{v_M^2 \, \pi} \right)^{3/2} \frac{1}{t^3} \exp \left(- \frac{r^2}{v_M^2 \, t^2} \right) \tag{4}$$

This distribution is a Gaussian with half-width increasing with the square of time and amplitude decreasing with t^3, the half-width is given by

$$r_g = v_M \, t$$

(b) Expansion of Cloud of Particles with Initial Maxwell Velocity Distribution From a Point Under a Linear Drag Law. - In this development, care must be taken to distinguish between the velocity distributions as a function of time. The defining equations are:

$$\frac{dv}{dt} = - cv \tag{5}$$

$$v = v_o \exp (- ct) \tag{6}$$

$$r = v_o/c \, [1 - \exp (-ct)] \tag{7}$$

For a small variation in initial velocity there is obtained

$$\delta r = \frac{\delta v_o}{c} [1 - \exp(-ct)] \qquad (8)$$

To obtain the velocity distribution, we consider a spherical shell at distance r from the origin and thickness δr at time t. The volume of this shell is given by

$$\delta v = 4\pi r^2 \delta r = 4\pi r^2 \delta_v \, 1/c \, [1 - (\exp(-ct)] \qquad (9)$$

Those particles where velocity v_o is such that they reach a distance r in time t are given by Equation (7) by some manipulations

$$v_o = \frac{r c}{[1 - \exp(-ct)]} \qquad (10)$$

Consequently putting Equation (10) in Equation (3) and dividing it by Equation (9), we obtain:

$$\rho(r,t) = \frac{N\left(\frac{1}{\pi v_M^2}\right)^{3/2} 4\pi\left(\frac{r c}{[1 - \exp(-ct)]}\right)^2 \exp - \left[\frac{r^2 c^2}{v_M^2 [1 - \exp(-ct)]}\right]^2}{4\pi r^2 \delta v \, 1/c \, [1 - \exp(-ct)]} \delta v$$

$$\rho(r,t) = N\left(\frac{1}{\pi v_M^2}\right)^{3/2} \frac{c^3}{[1 - \exp(-ct)]^3} \exp - \left[\frac{r^2 c^2}{v_M^2 [1 - \exp(-ct)]^2}\right] \qquad (11)$$

This is a Gaussian distribution of half-width $r_g = v_M/c \, [1 - \exp(-ct)]$

for $ct \ll 1$ Equation (11) is identical with Equation (4)

for $ct \gg 1$ an asymptotic solution is obtained

$$\rho(r,t) = N\left(\frac{1}{\pi v_M^2}\right)^{3/2} c^3 \exp - \left[\frac{c^2}{v_M^2} r^2\right] \qquad (12)$$

This is equivalent to the free expansion at $t = 1/c$. However, it is established to a reasonable degree of approximation for $t \sim 3/c$ [$\exp(-3) = 0.05$]. This second approximation implies a fairly well defined limiting size of the cloud.

(c) Expansion of Cloud of Particle with Initial Maxwell Velocity Distribution from a Point Under a Square Drag Law. - The governing equations are

$$\frac{dv}{dt} = - c\, v^2 \tag{13}$$

$$v = \frac{v_o}{1 + c\, v_o t} \tag{14}$$

$$r = 1/c\ \ell n(1 + c\, v_o\, t),\ \ell^{rc} = 1 + c\, v_o\, t$$

$$v_o = 1/ct\ [\exp(-rc) - 1] \tag{15}$$

$$\delta r = t\, \exp(-rc)\, \delta v \tag{16}$$

Following the same procedure as in Equation (4), there is obtained the density function

$$\rho(r,t) = N\left(\frac{1}{\pi\, v_M^2}\right)^{3/2} \exp(-rc) \left(\frac{\exp(-rc) - 1}{r\, c}\right)^2 \frac{1}{t^3} \exp - \left[\left(\frac{e^{rc}-1}{ct}\right)^2 \frac{1}{v_M^2}\right] \tag{17}$$

The distribution is no longer Gaussian because of the term containing r in front of the exponential. The half-width is given by

$$r_g = 1/c\ \ell n\ (1 + v_M\, ct) \tag{18}$$

It is noted that for all three cases, the "half-width" at time t is determined by the distance the particle with the most probable velocity has travelled.

Density of Cloud of Particles Expanded from a Cylinder with Velocity Determined by Rotation of Cylinder. - This analysis is devoted to the conversion of cylindrically created initial velocity distributions with no drag, linear velocity drag force, and squared velocity drag force.

(a) Free Expansion with No Drag. - For a cylinder of radius R, length 1, containing N particles, the number of particles in an anmiles of width δr distance r from the center is given by:

$$dN(r) = \frac{N}{\pi R^2 1} \cdot 2\pi\, r\ell\, dr = 2N/R^2\ r\ d\ r\ \eta(r-R) \tag{19}$$

for

$r - R < o \quad \eta = 1$

$r - R > o \quad \eta = o$

Assuming the velocity is proportional to r, with ω the angular velocity

$$v = r\omega \text{ up to } r = R \tag{20}$$

or

$f = v/\omega$ and $dr = dv/\omega$ substituting in Equation (19)

$$dN(v) = 2N/(\omega R)^2\ v\ dv\ \eta\ (v-R\omega) \tag{21}$$

There is now considered the density distribution resulting from this initial velocity distribution. These particles which reach a shell at distance r (now r is used to describe all space and is greater than R. Also essentially the cylinder has been collapsed to a line) are determined by

$$r = vt \text{ or } v = r/t$$

$$dv = \frac{dr}{t} \tag{22}$$

Moreover, the shell's volume dV is given by

$$dV = 2\,\pi\ r\ 1\ dr \tag{23}$$

Consequently

$$\rho(r,t) = \frac{dN(v)}{dV} = \frac{\frac{2N}{(\omega R)^2} v\, dv\, \eta(v-R\omega)}{2\pi r\, 1\, dr} \tag{24}$$

Substituting Equation (22) and Equation (23) in Equation (24), there is obtained

$$\rho(r,t) = \frac{N}{\pi(\omega R)^2\, 1}\; 1/t^2\; \eta(r-R\omega t) \tag{25}$$

This gives a constant distribution up to the edge of the cloud, $R\omega t$.

(b) Expansion with Drag Proportional to Velocity. - Here the identical procedure is followed substituting Equation (7) and Equation (8) into Equation (21) to obtain

$$\rho(r,t) = \frac{N}{\pi\, 1\, (\omega R)^2}\; \frac{c^2}{(1-e^{-ct})^2}\; \eta\,[r-R\omega/c\,(1-e^{-ct})] \tag{26}$$

It is noted that similar to the free expansion case a constant distribution occurs with however a different time behavior. Moreover for ct small Equation (26) reduces to the free-molecular formula Equation (25). The bounded nature of the distribution is indicated by the η function which cuts off the distribution sharply.

(c) Expansion with Drag Proportional to Square of Velocity. - Here by putting (Equation (16) and Equation (15) into Equation (21) and dividing by Equation (23) there is obtained

$$\rho(r,t) = \frac{N}{\pi\, 1\, (\omega R)^2}\; \frac{1}{t^2}\left[\frac{e^{rc}(e^{rc}-1)}{rc}\right] \eta\,\{r - [1/c\; \ell n(1 + CR\,\omega\, t)]\}$$

This is no longer a constant distribution in space. The function containing r which gives this radial distribution is monotonic increasing from r = o to the maximum distance $r_{max} = 1/c\; \ell n(1 + CR\,\omega\, t)$ and has respectively the values at these points of 1 and

$$\frac{(1 + CR\,\omega\, t)\; C^2\; R\omega t}{\ell n(1 + CR\,\omega\, t)}$$

Effect of Velocity of Canister on Density Distribution

The effect of canister velocity ω on the preceding calculated distributions is pointed out in the following discussion. In general, the most convenient formulae are those around a "guiding center".

Isotropic Maxwell Distribution. -

(a) No Drag. - Since the velocity distribution and the particle density remain unchanged around the canister position the original calculated density distribution remains unchanged. However, it now must be referred to a moving center which is a distance $R = \omega t$ from the explosion point. This can also be expressed analytically in terms of a fixed coordinate system as

$$\rho(r,u,t) = N(1/\pi v_T^2)^{3/2}\ 1/t^3\ \exp - [1/v_T^2 t^2\ (r^2+\omega^2 t^2-2r\omega t \cos\theta)]$$

where

u = canister velocity and is along X-axis

θ = usual polar coordinate and the origin is along the point of release.

(b) Drag Proportional to Velocity. - Here is presented an intuitive evaluation of the formulae.

It can be seen, using a triangle for calculating the distance, that r is proportional to the vector sum of velocities with the constant of proportionality $1/c(1-e^{-ct})$. Consequently, if we now consider a moving origin whose distance from the fixed original origin is given as

$r = u/c(1-e^{-ct})$, about this center the density distribution is the same as about the fixed origin where $u = o$.

(c) Drag Proportional to V^2. - The formula is merely presented

$$\rho(r,\alpha,t) = N(\beta/\pi)^{3/2}\ e^{ct}/r^2 1\ \frac{(e^{ct}-1)^2}{C^2\omega^2 t^2 - 2C\omega t(e^{ct}-1)\cos\alpha + (e^{ct}-1)^2}$$

$$\times\ 1/C^2t^2\ (e^{ct}-1-C\omega t\cos\alpha)^2$$

Cylindrical Release with Linear Velocity Distribution. -

(a) No Drag. - The solution here is the same as with $\omega = o$, however, this distribution is now centered about the point $r = ut$.

(b) With Linear Drag. - The solution here is the same as with $\omega = o$, however, the distribution is now centered about the point

$$r = u/C(1-e^{-ct})$$

This result is valid independent of the angle between u and l.

(c) Drag Proportional to v^2. - The distributions now depend on u and θ.

ABSTRACTS OF PAPERS SUPPORTED COMPLETELY OR IN PART FROM THIS CONTRACT

A Spectroscopic Study of The Chemiluminescent Reaction of Germanium Tetrahydride With Atomic Oxygen (Accepted for Publication in Proc. Phys. Soc. London, January 1967) By A. Sharma and J. P. Padur

The spectrum of the glow produced during the gas phase reaction of germanium tetrahydride with atmoic oxygen is studied in the region from 2450 to 5100Å. About one hundred bands are measured between 2350 and 4000Å. The initial spectrum was recorded with a Perkin-Elmer (Model 99) monochromator equipped with a 600 line/mm grating and the final spectrum was photographed with 1.5 m Jarrel-Ash grating spectrograph. Most of the bands belonging to the D-X system of GeO observed by previous workers are identified in the present spectrum. A number of new bands belonging to the D-X system of GeO observed by us for the first time were identified after calculating their band heads from the following formula:

$$\nu = 37762.4 + (651.3v' - 4.2v'^2) - (985.7'' - 4.3v''^2)$$

where $u = v + 1/2$

A number of additional bands found could not be ascribed to the above band system and indicate the presence of a new band system of GeO. Most of these bands lie between 3000 and 3800Å. The spectrum was also photographed with a Hilger's small quartz spectrograph which has larger light gathering power but low dispersion. This spectrum shows the presence of additional bands in the region between 4000 and 5000Å. This observation substantiates the presence of a new band system of GeO on the longer wavelength side of the D-X system. The possibility of a new band system of GeO is also indicated from the comparison of the observed band systems belonging to the diatomic oxides of the elements of the IV-a group of the periodic table (CO, SiO, GeO, SnO and PbO).

The True Potential Energy Curves of $X^2\Sigma$ and $A^2\Sigma$ State of The AℓO Molecule (Accepted for publication in J. Quant. Spectrosc. Rad. Transfer) By A. Sharma

The reliable interpretation of the relative intensity of the bands belonging to the $A^2\Sigma - X^2\Sigma$ system of AℓO observed during the rocket release of aluminum compounds in the upper atmosphere at twilight in terms of upper atmospheric temperature requires accurate Franck-Condon factors. The Franck-Condon factors fo for the above band system have previously tested after assuming that the $A^2\Sigma$ and $X^2\Sigma$ states follow the Morse curve. It has also been found that Franck-Condon factors are quite sensitive to the shape of the potential energy curve. Therefore, investigation concerned whether the shape of the potential follows the Morse curve. For the case of Morse curve, the following relation between spectroscopic constants holds

$$\alpha_e = 6\sqrt{\frac{\omega_e x_e B_e^3}{\omega_e}} - 6\frac{B_e^2}{\omega_e}$$

The value of α_e calculated from the above relation was compared with the experimentally measured one. It was found that the agreement between two values is good for $X^2\Sigma$ state, but the two values show large difference from $A^2\Sigma$ state.

In view of the above finding, the true potential energy curves of $X^2\Sigma$ and $A^2\Sigma$ states were calculated by Rydberg-Klein-Rees method. The true potential energy curves were then graphically compared with those of corresponding Morse curve. The above comparison showed that the agreement between the true potential and Morse potential is reasonable for $X^2\Sigma$ state – particularly for $v\leq 6$. However, the deviation of the true potential for $A^2\Sigma$ state from the corresponding Morse potential is appreciable for even lower vibrational levels.

The Franck-Condon Factors and R-Centroids of $A^2\Sigma$ - $X^2\Sigma$ Band Systems of AlO (Accepted for Publication in J. Quant. Spectrosc. and Rad. Transfer) By A. Sharma

It is well known that the reliable estimates of the upper atmospheric temperatures require accurately calculated Franck-Condon factors. Previous workers have calculated the Franck-Condon factors after assuming that $X^2\Sigma$ and $A^2\Sigma$ states of AlO follow the Morse curve. However, we have shown that although the difference between the true potential and the corresponding Morse potential is not large for $X^2\Sigma$ state, but is rather appreciable for $A^2\Sigma$ state. Since it has been found that the values of Franck-Condon factors are rather sensitive to the shape of the potential, we have calculated the Franck-Condon factors and the R-centroids from the true potentials. The relevant wave functions were obtained from the numerical integration of the following Schrödinger equation:

$$\frac{d^2\psi(v)}{dr^2} + [E(v) - u(v)]\,\psi(v) = 0$$

after substituting the true potential energy curves for u(r) which were calculated by us.

The accuracy of the calculated true potentials were tested by comparing the calculated eigen-values E (v) with the observed g(v) values. It was found that for $v\leq 7$ for the two states the agreement was within the accuracy of the presently available data. However, larger deviation was found for 8th and 9th vibrational levels of the two states – particularly the 9th vibrational level of $X^2\Sigma$ state, which was due to the inaccuracy of the experimental data. A further check on the accuracy of the true potential curves was made by comparing the theoretically calculated B(v) values with those found from the rotational analysis of the corresponding band. Again, the agreement between the two values for the two state was within the accuracy of the experimental data.

The Franck-Condon factors and r-centroids calculated from the true potentials were compared with those previously calculated from the Morse potentials. The maximum difference between the Franck-Condon factors calculated from the two potentials for prominent bands [$g(v', v'')>0.1$] is up to 50 percent. However, the value of the Franck-Condon factors calculated from the two potentials for weak bands differ even in order of magnitude.

It was also found that the difference between the r-centroids calculated from the two potentials is of the same order of magnitude. The applicability of the recent graphical method of Jaunes for obtaining the r-centroid values of a band system was also tested.

Studies of Ion-Molecule Reactions by a Photoionization Mass Spectrometer Technique by Peter Warneck

A photoionization mass spectrometer has been used for ion-molecule reaction studies. Ion source pressures up to 200 microns are employed, measured directly with a McLeod guage. This investigation differs from previous mass spectrometer investigations of ion-molecule reactions in two respects: (1) photoionization replaces the more commonly employed electron impact mode of ion formation, and (2) a new technique is employed for the determination of ion residence times in the source in the presence of a constant repeller field. The ensuing advantages are: first, the state of the primary ions is reasonably well defined by the choice of ionizing wavelength, and second, the residence times can be obtained without a detailed knowledge of the electric field configuration in the ion source. This is particularly valuable at higher pressures where residence times are not calculable from Newton's formula. The interpretation of ion pulse shapes in terms of ion density distributions enables the determination of ion of ion diffusion coefficients from the broadening of the density profile, and ultimately the derivation of approximate ion temperatures. It is an important finding that at pressures about 50 microns, where the basic motion of ions is drift in the electric field, the ionic temperatures are in the thermal range provided only moderate fields are applied.

Rate constant values have been determined for the reactions.

(1)	$N_2^+ + O_2 \rightarrow O_2^+ + N_2^+$	$k_1 = 1.1 \times 10^{-10}$	cc/molecule sec
(2)	$N_2^+ + O_2 \rightarrow NO^+ + NO$	$k_2 < 3 \times 10^{-14}$	cc/molecule sec
(3a)	$N_2^+ + 2N_2 \rightarrow N_4^+ + N_2$	$k_{3a} = 8.5 \times 10^{-29}$	$cc^2/molecule^2$ sec
(4)	$H_2^+ + H_2 \rightarrow H_3^+ + H$	$k_4 = 1.85 \times 10^{-9}$	cc/molecule sec

Satisfactory agreement is obtained in all cases where previous values are available for comparison, indicating that the methods applied here are useful in extending rate constant determinations towards higher pressures than previously applied.

The Chemiluminescent Reactions of Atomic Oxygen with COS and H_2S

(A. Sharma, J.P. Padur, and P. Warneck)

The chemiluminescence intensity in the reactions of O + COS and O + H_2S was studied in a flow system as a function of reaction time and reactant concentrations. In the initial stage of the reactions, the intensity increases linearly with time, the slope being proportional to the concentration of COS or H_2S and to the square of atomic oxygen concentration. A kinetic analysis shows that these results are consistent with the notion that the reaction responsible for the emission in both cases is

$$(1) \quad O + SO \rightarrow SO_2 + h\nu$$

From the relative intensities the rate of SO formation in the H_2S reaction was found to be 1.85 times greater than that in the COS reaction. It was further ascertained that in the 300 to 800 micron pressure region reaction (1) is pressure dependent. Also, the bimolecular rate constant, obtained at 800 microns by comparison with the emission from the reactor O + NO, was found to be greater by an order of magnitude than that reported previously for much smaller pressures. Finally, the emission intensity in the late stages of the O + COS reaction has been measured to determine the extent of SO consumption. It is concluded that other SO loss reactions must be operating in addition to reaction (1).

Studies of Ion-Neutral Reactions by a Photoionization Mass Spectrometric Technique

(Peter Warneck)

Several positive ion-neutral reactions of importance in the ionosphere have been investigated with the photoionization mass spectrometer technique developed in this laboratory (P. Warneck, J. Chem. Phys., in press). This new method utilizes photionization for the production of primary ions in a mass spectrometer ion source, and the reactions that these ions undergo during their sojourn to the extraction orifice as studied from the decay of the primary ion intensity and increase of secondary ion intensity as measured at the mass spectrometric detector. A new technique, utilizing a pulsed ion source is applied to determine directly the residence time of the primary ions in the ion source, so that rate constant determinations can be made. The reactions studied and the associated measured rate coefficients (in cc/sec) are

$$(1) \quad O^+ + O_2 \rightarrow O_2^+ + O \qquad k_1 = 2.0 \pm 0.5 \times 10^{-11}$$

$$(2) \quad O^+ + N_2 \rightarrow NO^+ + N \qquad k_2 = 4.6 \pm 1.1 \times 10^{-12}$$

$$(3)\quad N_2^+ + O_2 \rightarrow O_2^+ + N_2 \qquad k_3 = 1.1 \pm 0.2 \times 10^{-10}$$

$$(4)\quad O_2^+ + N_2 \rightarrow NO^+ + NO \qquad k_4 = 3 \times 10^{-15}$$

$$(5)\quad N^+ + O_2 \rightarrow O_2^+ + N \qquad k_5 = 4.8 \pm 1.6 \times 10^{-10}$$

$$(6)\quad N^+ + O_2 \rightarrow NO^+ + O \qquad k_6 = 1.9 \pm 0.7 \times 10^{-10}$$

$$(7)\quad O_2^+ + NO \rightarrow NO^+ + O_2 \qquad k_7 = 7.7 \pm 1.5 \times 10^{-10}$$

None of the determined rate coefficients shows any signs of a temperature dependence. The obtained rate data and in good agreement with values by other workers using different methods.

The Morphology of Intermediate Optically Thick Chemical Release Clouds

(See Quarterly Progress Report Number Three
J. Pressman and H.K. Brown)

This study was undertaken to rationalize the morphology of intermediate optically thick chemical release clouds. In this range of opacity (τ = 1-10) The cloud can take on a large variety of shapes. The study makes use of a geometrical approach as an approximative technique. In this approach, a region of one optical unit thickness is demarcated into which light can penetrate from the source. In another region, one optical unit thickness is demarcated along the line of sight from which light can emerge to the observer. It is the intersection of these two regions that forms the image. A simple graphical technique has been developed for determining the visible image and images have been drawn for a wariety of optical thicknesses and phase angles. Analytical solutions have also been determined, but in general, because of the complexity of the shapes, they are cumbersome. From the shape of the image one can work backward and determine the optical thickness of the cloud.

The Dispersion of Particulate Matter in the Upper Atmosphere for Different Initial Velocity Distribution and Drag Laws

(J. Pressman and H.K. Brown)

This is a mathematical study of the dispersion of particulate matter in the upper atmosphere under different initial velocity distributions for the particles and for different drag laws. Its purpose is to provide a framework for the design and analysis of such experiments. Its thesis is that by knowing the initial velocity distribution and the drag law this particle space distribution can be determined at any time. In practice, from the mathematical results of the study, a canister design and release pressure will be engineered to

achieve a desired velocity distribution of particles. The cloud images then will be compared with that due to the prescribed velocity distribution interacting with the atmospheres under different drag laws to establish what the drag laws are for particles of the size used at the altitude of release.

The velocity distributions considered are constant, linear, and Maxwell. The drag laws considered have been constant, linear, and square. The various permutations of these two factors have been included with the additional parameter of canister motion – either no velocity or a prescribed velocity.

On the Chemiluminous Reaction of Atomic Oxygen and Nitric Oxide (To be Published)

(A. Sharma and J. Pressman)

The elucidation of the mechanism of the chemiluminous reaction of atomic oxygen with nitric oxide is of importance for the understanding of the glow produced by the rocket release of nitric oxide in the upper atmosphere and the emission of the night airglow continuum. The available laboratory data is critically evaluated. In veiw of relatively long lifetime of excited NO_2 molecule ($\sim 4.4 \times 10^{-5}$ sec), the effect of wall quenching was found to be appreciable and had not been previously taken into consideration. However, the discrepancy between the rate coefficient of the chemiluminous reaction determined in the laboratory ($\sim 10^{-17}$) c^3 $molecule^{-1}$ sec^{-1}) and that obtained from the rocket and wind tunnel experiments (10^{-13} cm^3 mol^{-1} sec^{-1}) is not understood. It should, however, be pointed out that the only quantitative measurement of the rate constant of the chemiluminous reaction is in Hg pressure region. A measurement of the above rate constant should be independently be made in lower pressure region.

Spectroscopic and Fluorescent Studies of the Chemiluminescent Reaction of Triethyl Boron with Atomic Oxygen (To be Published)

(A. Sharma, ShardaNand and J.P. Padur)

Since the twilight and the night time release of triethyl boron in the upper atmosphere has been proposed by GCA, the spectroscopic and fluorescent studies of the thriethyl boron with atomic oxygen were carried out. The spectrum of the glow produced during the above reaction was recorded with a Perkin Elmer (Model 99) monochromator equipped with a 600 line/mm grating and was also studied photographically. The spectrum of the glow predominantly consists of BO_2 bands, however, the presence of some bands belonging to the α and β systems of BO is also indicated.

The fluorescence of the reacting gases was studied so that some information regarding the population of unexcited intermediate products could be obtained. The fluorescence was excited by the light from a high pressure Xenon arc lamp (Osram XBO, 1600 watt). The total pressure in the reaction cell was

about 1 mm Mg. A definite enhancement of a band around 5450Å was observed and was found to be due to the resonance fluorescence. The observed band at about 5450Å is identified as the (0, 0, 0 __ 0, 0, 0) band of the $A^2\pi_u$ $X^2\pi_g$ system of BO_2. This observation indicated that the appreciable concentration of unexcited BO_2 is present as an intermediate product in the reaction system.

The effect of the atomic oxygen concentration on the intensity of the chemiluminescence and also on the fluorescent enhancement was investigated. It was found that the intensity of the chemiluminescence is directly proportional to the atomic oxygen concentration. However, the effect of the atomic oxygen concentration variation on the fluorescent enhancement of the BO_2 band is about one fifth of its effect on the intensity of chemiluminescence.

REFERENCES

1. Liuti, G., S. Dondes and P. Harteck, presented at the Fall Meeting of the American Chemical Society, New York(1963).

2. Sullivan, J.O. and P. Warneck, Ber. Bunsenges. 69, 7 (1965).

3. Sharma, A., J.P. Padur and P. Warneck, J. Chem. Phys. 43, 2155 (1965).

4. Gaydon, A.G., "The Spectroscopy of Flames," Chapman and Hall, Ltd, London (1957).

5. Hermann, L., J. Akrich and M. Grenat. Spectry. Radiative Transfer 2, 215 (1962).

6. Halstead, C.J., B.A. Thrush, Nature 204, 992 (1964).

7. Rolfes, T.R., R.R. Reeves and P. Harteck, J. Phys. Chem. 69, 849 (1965).

8. Gaydon, A.G., Spectroscopy of Flames, John Wiley and Sones, Inc., New York (1957).

9. Kaufman, F., Progress in Reaction Kinetics, Part I, Edited by Porter, Pergamon Press, New York (1961).

10. Jevons, W., L.A. Bashford, and H.V.A. Briscoe, Proc. Phys. Soc. 49, 543-53 (1937).

11. Authier, B., Ann. Geophysique 20, 353 (1964).

12. Harrang, O., Planet. Space Sci. 12, 567 (1964).

13. Authier, B., J.E. Blamont and G. Carpenter, Ann. Geophysique 20, 342 (1964).

14. Nicholls, R.W., J. Res. Natl. Bur. Stand. 66A, 227 (1962).

15. Tawde, N.R. and V.M. Korwar, Proc. Phys. Soc. Lond. 80, 794 (1962).

16. Zare, R.N., E.O. Larson and R.A. Berg, J. Mo. Spectrosc. 15, 117 (1965).

17. Authier, A.B., Ann Geophys, 20, 353 (1964).

18. Harrang, O, Planet Space Sci, 12, 567 (1964).

19. Authier, B., J.E. Blamont and G. Carpenter, Ann Geophys. 20, 342 (1964).

20. Nicholls, R.W., J. Res. Nat'l Bur Stand, 66A, 227 (1962).

21. Tawde, N.R. and V.M. Korwar, Proc Phys Soc Lond 80, 794 (1962).

22. Sharma, A. JQSRT, to be published.

23. Zare, R.N., E.O. Larson and R.A. Berg, J. Mol Spectrosc, 17, 117 (1965).

24. Tawde, N.R. and S.A. Trivedi, Proc. Phys. Soc., 51, 733 (1939).

25. Robinson, D. and R.W. Nicholls, J. Quant. Spectrosc. Radiative Transfer 1, 76 (1961).

26. Tawde, N.R. and V.M. Korwar, Proc. Nat. Inst. Sci. (India) 29, 325 (1963).

27. Herbert, G.R. and Tyte, D.C., Proc. Phys. Soc. 83, 629 (1964).

28. Tyte, D.C. and G.R. Herbert, Proc. Phys. Soc. 83, 830 (1964).

29. Harang, O., Planet Space Sci. 12, 567 (1964).